Available online at www.sciencedirect.com
SCIENCE DIRECT®
Electrochemistry Communications 5 (2003) 124–128
electrochemistry communications
www.elsevier.com/locate/elecom

Synthesis and electrochemical properties of sulfur doped-$Li_xMnO_{2-y}S_y$ materials for lithium secondary batteries

Sang-Ho Park [a], Yun-Sung Lee [b], Yang-Kook Sun [a,*]

[a] Department of Chemical Engineering, Hanyang University, Seoul 133-791, South Korea
[b] High-Tech Research Center, Kanagawa University, Yokohama 221-8686, Japan

Received 11 December 2002; received in revised form 6 January 2003; accepted 6 January 2003

Abstract

Sulfur doped lithium manganese oxides ($Li_xMnO_{2-y}S_y$) were prepared by ion exchange of sodium for lithium in $Na_xMnO_{2-y}S_y$ precursors obtained by a sol–gel method. These materials had the nano-crystallite size, which was composed of grain size of about 100–200 nm. Especially, $Li_{0.56}MnO_{1.98}S_{0.02}$ delivered the initial discharge capacity of 170 mAh g^{-1} and gradually increased the discharge capacity of 220 mAh g^{-1} until 50 cycles. Moreover, it showed an excellent cycling behavior, although its original structure transformed into the spinel phase during cycling.

Keywords: Lithium-ion battery; Sulfur doping; Layered manganese oxide; Sol–gel method; Nano-crystallite size

1. Introduction

The lithium manganese oxide has been great attention as a promising cathode material for lithium secondary batteries because of its comparatively low cost and low toxicity [1,2]. Recently, the layered $LiMnO_2$ with the O3 (α-$NaFeO_2$) structure has been actively studied due to its high theoretical discharge capacity of 285 mAh g^{-1}, which is nearly twice that of spinel $LiMn_2O_4$. However, direct synthesis of layered $LiMnO_2$ material is not possible because the non-layered structures $LiMn_2O_4$ (spinel), $LiMnO_2$ (orthorhombic), or Li_2MnO_3 (monoclinic) are more stable than layered structure. The layered $LiMnO_2$ was observed to undergo a detrimental phase transformation to a spinel-like phase during the first removal and subsequent cycling of lithium ions, leading to eventual degradation of electrode performance [3–5]. However, an ion exchange method has been applied to the preparation of layered lithium manganese oxide. Paulsen et al. [6,7] reported that the high temperature O2-type $Li_{0.7}[Ni_{1/3}Mn_{2/3}]O_2$ prepared by ion exchange Li for Na from the P2-type $Na_{0.7}[Ni_{1/3}Mn_{2/3}]O_2$ showed a large capacity of about 180 mAh g^{-1} with good capacity retention, and did not transform to spinel on electrochemical cycling. Quine et al. [8] reported that although m-$Li_xMn_{0.95}Ni_{0.05}O_2$ prepared by ion-exchange of $NaMn_{0.95}Ni_{0.05}O_2$ delivered a reversible capacity retention of 200 mAh g^{-1} between 4.8 and 2.4 V, the material transformed slowly to a spinel-like material during cycling. In order to further stabilize the layered structure, Mn-substituted $LiMn_{1-y}M_yO_2$ (M = Al, Cr, Co, Ni, Li, Ti, Mg) has been widely studied [5–9]. Meanwhile, Kubo and Naghash et al. [10–12] are reported that crystal structure of the material was stabilized by partial substituting fluorine for oxygen in $LiNiO_2$. Recently, we reported that anion doping with sulfur was very effective in stabilizing the crystal structure and electrochemical properties of $LiMn_2O_4$ and $LiNiO_2$ [13,14].

In this work, we have attempted $Li_xMnO_{2-y}S_y$ ($y = 0$, 0.1, 0.2 and 0.3) materials through ion exchange of Li for Na from the $Na_{0.7}MnO_{2-y}S_y$ precursor prepared by a sol–gel method. We investigate the effect of the amount of sulfur doping in the $Li_xMnO_{2-y}S_y$ materials on the electrochemical performance.

* Corresponding author. Fax: +82-2-2282-7329.
E-mail addresses: yksun@hanyang.ac.kr, saga98ts32@yahoo.co.jp (Y.-K. Sun).

1388-2481/03/$ - see front matter © 2003 Published by Elsevier Science B.V.
doi:10.1016/S1388-2481(03)00005-5

2. Experimental

$Na_{0.7}MnO_{2-y}S_y$ precursor was synthesized using a sol–gel method. $NaCH_3COO$, $Ni(CH_3COO)\cdot 4H_2O$, $Mn(CH_3COO)_2\cdot 4H_2O$ and Na_2S salts were dissolved in distilled water. The dissolved solution was added dropwise to a continuously stirred aqueous solution of glycolic acid as a chelating agent. The molar ratio of chelating agent to total metal ions was fixed in unity. The pH of the solution was adjusted to be in the range of 8–9 by adding ammonium hydroxide. The resultant solution was evaporated at 80 °C until a transparent sol and gel was obtained. The resulting gel precursors were decomposed at 450 °C for 5 h in air, calcined at 600 °C in air for 12 h, and then quenched to a room temperature.

The prepared precursor, $Na_{0.7}MnO_{2-y}S_y$, was introduced into a mixed solution of ethanol and LiBr. The ion exchange of sodium for $Na_{0.7}MnO_{2-y}S_y$ with lithium was carried out at 80 °C for 3 h in the mixed solution using a batch reactor equipped with a reflux condenser to prepare $Li_xMnO_{2-y}S_y$ material. After the reaction, the solution was filtered using a vacuum suction filtering equipment and the remaining powder was washed with distilled water and ethanol. The washed powders were dried at 180 °C for 24 h in a vacuum oven.

After the synthesis, the amounts of Li, Mn and S in the synthesized materials were analyzed with an inductively coupled plasma (ICP) and sulfur analyzer (LECO, CS 444), respectively, to determine the real chemical composition of the materials. Powder X-ray diffraction (XRD, Rint-2000, Rigaku, Japan) using CuKα radiation was used to identify the crystalline phase of the resulting material. Rietveld refinement was then performed on the XRD data to obtain lattice constants. Crystallite size of the particles was calculated from the XRD pattern by Scherrer's equation [15]. The grain size and morphology of the compounds were observed using a field emission scanning electron microscope (FE-SEM, JEOL, Japan).

The electrochemical properties of the synthesized powder were performed in CR2032 coin type cells. The cathode was fabricated with 20 mg of accurately weighed active material and 12 mg of conductive binder (8 mg of Teflonized acetylene black (TAB) and 4 mg of graphite). It was pressed on a 250 mm^2 stainless steel mesh used as the current collector at a pressure of 300 kg cm^{-2} and dried at 200 °C for 5 h in an oven. The test cell was made of a cathode and a lithium metal anode (Cyprus Foote Mineral) separated by a porous polypropylene film (Celgard 3401). The electrolyte used was a mixture of 1 M $LiPF_6$-ethylene carbonate (EC)/dimethyl carbonate (DMC) (1:2 by volume). All the assembling of the cell was carried out in an argon-filled dry box. The charge and discharge cycling was performed at a current density of 0.4 mA cm^{-2} with a cut-off voltage of 2.0–4.6 V (vs. Li/Li^+) at room temperatures.

3. Results and discussion

Fig. 1 shows the X-ray diffraction (XRD) patterns of the prepared $Li_xMnO_{2-y}S_y$ ($y = 0$, 0.1, 0.2, and 0.3) materials after ion-exchange reaction. All the XRD patterns of the materials appear to be a highly disordered, judging from the broadened peaks and containing high disorder diffraction. Increasing the doped-sulfur contents, the full width half maximum (FWHM) of the main peaks ($2\theta = 18.4°$) decreased due to the increase of crystalline sizes. Furthermore, the splitting of two (1 0 8) and (1 1 0) peaks at $2\theta = 64.2°$ and 64.7° was accelerating with the increase of doped sulfur contents. Therefore, we assumed that all the XRD patterns are indexed a typical layered structure without any impurity peaks in the whole range of sulfur doping contents.

The lattice constants, a and c, of the synthesized materials were calculated by the Rietveld refinement using the XRD data of Fig. 1. and real compositions are listed in Table 1. It shows that the lattice constants, a- and c-axes, vary smoothly with the sulfur content. The lattice constant of a-axis increases very slightly from 2.82 to 2.84 Å, whereas the lattice constant of c-axis increases slightly from 14.37 to 14.52 Å. This might cause the elongation of c-axis because the ionic size of sulfur is larger than that of oxygen. Furthermore, it was confirmed that the the typical XRD pattern of $Li_{0.56}MnO_{1.98}S_{0.02}$ materials has a small R_{wp} of 11.81% would show a successful refinement by Reitveld analysis [16]. From the result, we assumed that $Li_xMnO_{2-y}S_y$ materials in this study had the O3 hexagonal structure with space group of $R\bar{3}m$ (No. 166).

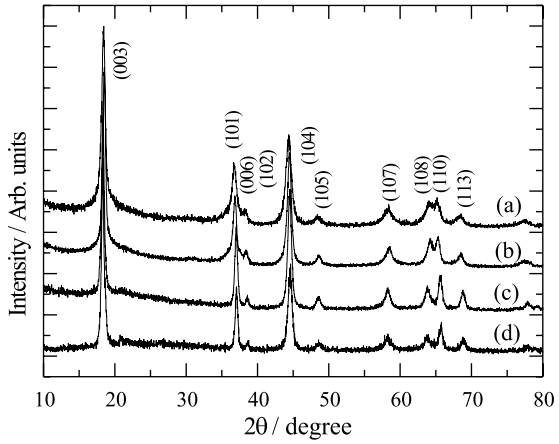

Fig. 1. X-ray diffraction patterns of: (a) $Li_{0.7}MnO_2$, (b) $Li_{0.7}MnO_{1.9}S_{0.1}$, (c) $Li_{0.7}MnO_{1.8}S_{0.2}$ and (d) $Li_{0.7}MnO_{1.7}S_{0.3}$ compounds.

Table 1
Lattice constants, lithium content and sulfur content measured by Rietveld analysis, ICP and sulfur analyzer, respectively

Nominal composition	Lattice constants		R_p (%)	R_{wp} (%)	R_{exp} (%)	Final Li contents (molar ratio)	Final S contents (molar ratio)	FWHM of (0 0 3) peak
	a (Å)	c (Å)						
$Li_{0.7}MnO_2$	2.82	14.37	9.23	12.15	2.46	0.55		0.723
$Li_{0.7}MnO_{1.9}S_{0.1}$	2.85	14.35	10.08	11.72	0.15	0.57	0.01	0.530
$Li_{0.7}MnO_{1.8}S_{0.2}$	2.84	14.46	11.81	13.08	0.33	0.56	0.02	0.482
$Li_{0.7}MnO_{1.7}S_{0.3}$	2.84	14.52	23.56	30.98	0.42	0.58	0.03	0.361

*R_p, pattern R-factor; R_{wp}, weighted pattern R-factor; R_{exp}, expected R-factor.

The morphology of the as-prepared powders was observed by means of scanning electron microscopy (SEM). Fig. 2(a) showed SEM photograph for $Li_{0.56}MnO_{1.98}S_{0.02}$ powders. Not Shown in this figure, all samples are an amorphous-like agglomeration. The average grain sizes of the powders are below 200 nm. Fig. 2(b) shown that the crystalline size was calculated by applying the values of FWHM of (0 0 3) peaks of Fig. 1 to the Scherrier's equation [15]. The crystalline size of $Li_xMnO_{2-y}S_y$ increases with the increase of the substituted amount of sulfur ions, which indicates the decrease of the FWHM of (0 0 3) peaks. In recent, it has been reported that the decrease of main peak width (0 0 3 direction) is attributed to an decrease of the homogeneous strains in the particles during the reaction [17]. It is might be assumed to be due to the catalytic activity of sulfur element in the synthetic process. Therefore, it has been experimentally considered that the nano-sized crystallites tend to improve electrochemical properties and enhance the structural stability during cycling [18,19].

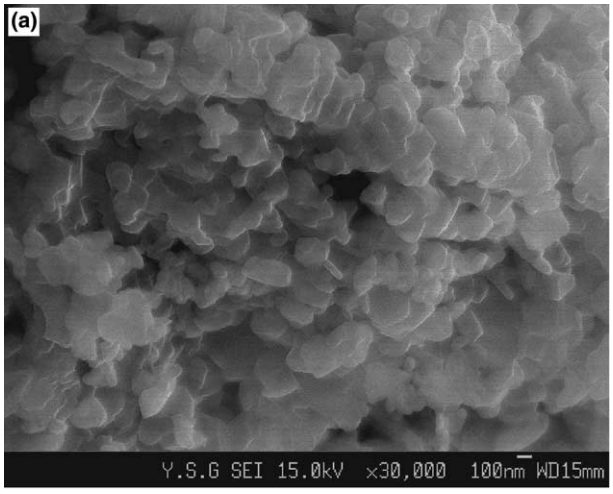

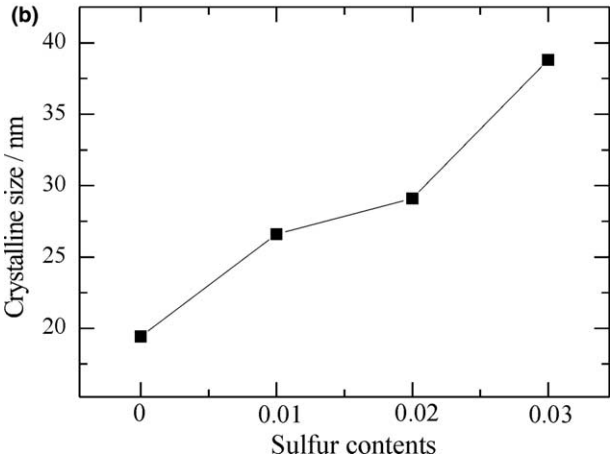

Fig. 2. (a) Scanning electron micrograph for $Li_{0.56}MnO_{1.98}S_{0.02}$ powder. (b) Crystallite size as a function of sulfur contents.

The variation in the specific discharge capacity with the number of cycles for the $Li/Li_xMnO_{2-y}S_y$ cells was shown in Fig. 3. The cycling behavior of $Li_{0.55}MnO_2$ electrode is also shown in this figure, in order to compare with that of $Li_xMnO_{2-y}S_y$ electrodes. Although $Li_{0.57}MnO_{1.99}S_{0.01}$ delivers the highest initial discharge capacity of 200 mAh g^{-1}, the capacity gradually decreases with the cycle number and exhibits apparent capacity loss after 50 cycles. However, the $Li_{0.56}MnO_{1.98}S_{0.02}$ material shows a relatively small discharge capacity of 170 mAh g^{-1} and still presents a high discharge capacity of 220 mAh g^{-1} after 50 cycles. Our previous works also revealed the similar behavior that the substitution of sulfur for oxygen is very effective in preventing the capacity loss at the lower potential range (3 V regions) due to the overcoming Jahn-teller distortion [13].

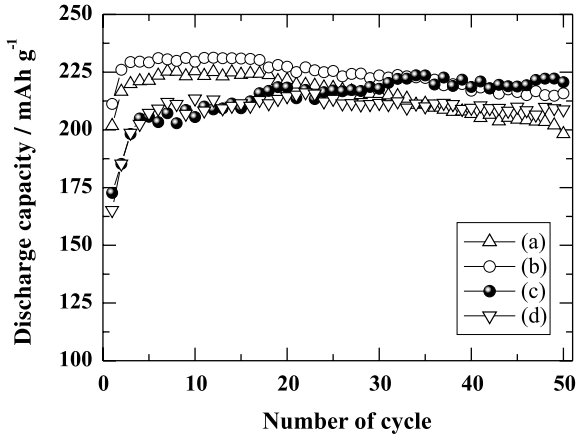

Fig. 3. Plots of discharge capacity vs. number of cycles for the $Li/LiPF_6$-EC/DMC (vol. 1:2)/$Li_{0.56}MnO_{2-y}S_y$ cells. (a) $y = 0$, (b) $y = 0.01$, (c) $y = 0.02$ and (d) $y = 0.03$.

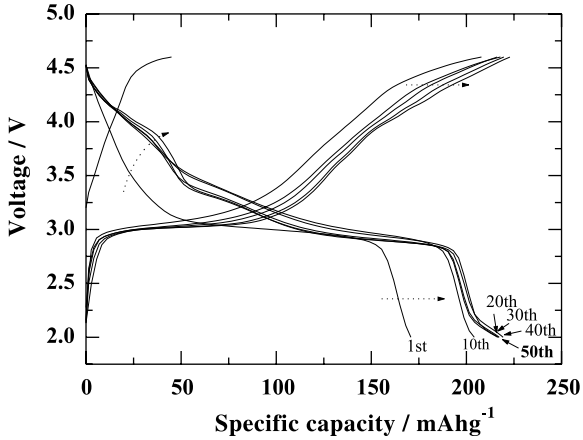

Fig. 4. Charge/discharge curves with the number of cycles for the Li/LiPF$_6$-EC/DMC(vol. 1:2)/$Li_{0.56}MnO_{1.98}S_{0.02}$ cell.

Fig. 4 shows the charge/discharge curves of the Li/$Li_{0.56}MnO_{1.98}S_{0.02}$ cell as a function of number of cycles. The first discharge curve exhibited a long plateau at about 3.0 V. The presence of plateau at 3.0 V is one characteristic of the Li_xMnO_2 (O3 type) materials and it also could be observed during the first a few cycles of orthorhombic $LiMnO_2$ material [5,8]. However, with further cycling, the voltage profile is starting to develop small another plateau at about 4.15 V. It is noticeable this 4 V plateau become increased and flattered on cycling. It is well known that the 4 V plateau is characteristics of the spinel ($LiMn_2O_4$) material, in which lithium ions are intercalated into the tetrahedral sites over the 4 V regions. Therefore, the presence of new plateau at 4 V strongly supports that $Li_{0.56}MnO_{1.98}S_{0.02}$ material in this study slowly transformed into a cubic spinel structure during cycling. Similar observation previously reported that the layered Li_xMnO_2 transformed to spinel phase during lithium ion intercalation and deintercalation [20,21].

Fig. 5 shows differential capacity vs. voltage of $Li_{0.56}MnO_{1.98}S_{0.02}$ electrode in the voltage region of 2.0–4.6 V. The differential capacity of $LiMn_2O_4$ is also presented in the inset of Fig. 5. Stoichiometric $LiMn_2O_4$ spinel has two clear reduction peaks at 3.95 and 4.1 V, which suggests the lithium ions are extracted and inserted into the spinel phase by two-step process [22]. However, $Li_{0.56}MnO_{1.98}S_{0.02}$ electrode at the 10th cycle has only one reduction peak at the same voltage region. The single reduction peak gradually divides into two reduction peaks after 30th cycle at around 4 V and one reduction peak is gradually increase after 30th cycle at about 3.3 V. We assumed that divided 4 V peaks and increasing 3.3 V reduction peaks of $Li_{0.56}MnO_{1.98}S_{0.02}$ electrode attributed to the transformation to spinel phase.

However, even if the $Li_{0.56}MnO_{1.98}S_{0.02}$ electrode was undergone the transformation to spinel during cycling, the Li/$Li_{0.56}MnO_{1.98}S_{0.02}$ cell showed not only a high initial capacity, but also an excellent cycle retention. The variation of the discharge capacity of Li/$Li_{0.56}MnO_{1.98}S_{0.02}$ cell in the 2.0–4.6 V range at various current densities (*C*-rate) is presented in Fig. 6. The discharge capacities of this cell slowly decreased with increasing current densities and were determined to be 215, 205 and 180 mAh g^{-1} at current densities of 0.2, 0.5 and 1 C, respectively. Furthermore, Li/$Li_{0.56}MnO_{1.98}S_{0.02}$ cell presented excellent capacity retention at various current densities.

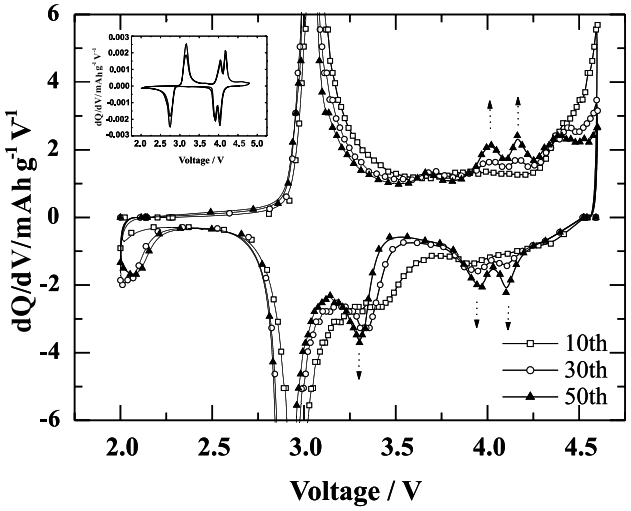

Fig. 5. Differential capacity vs. voltage for $Li_{0.56}MnO_{1.98}S_{0.02}$ electrode. This cell was tested between 2.0 and 4.6 V using a current density of 0.4 mA cm^{-2} (*C*/4).

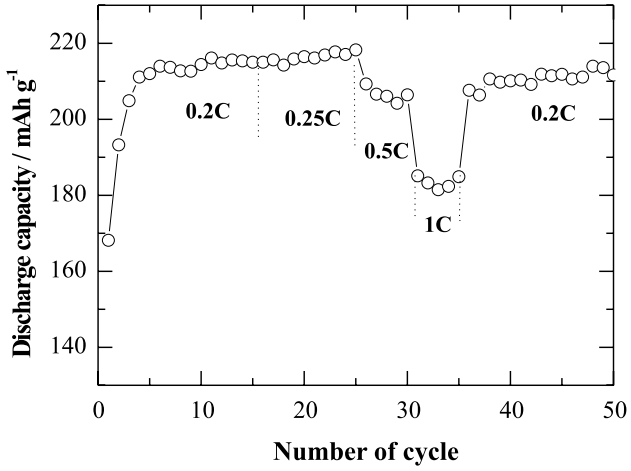

Fig. 6. Discharge capacity vs. number of cycles for the Li/$Li_{0.56}MnO_{1.98}S_{0.02}$ cell at various current densities.

4. Conclusion

Sulfur-doped lithium manganese oxides ($Li_xMnO_{2-y}S_y$) are prepared by ion exchange of sodium for lithium in $Na_{0.7}MnO_{2-y}S_y$ precursor synthesized by a sol–gel

method. The $Li_{0.55}MnO_2$ electrode initially delivered a high discharge capacity of 200 mAh g^{-1}, but the capacity gradually decreased with the electrochemical cycling.

Though, even if the $Li_{0.56}MnO_{1.98}S_{0.02}$ material delivered an initial discharge capacity of 170 mAh g^{-1}, the discharge capacity steady increased up to 220 mAh g^{-1} after 50 cycles in the 2.0–4.6 V. The voltage profiles and differential capacity data indicated that the $Li_{0.56}MnO_{1.98}S_{0.02}$ material gradually transforms to spinel structure during cycling. However, $Li_{0.56}MnO_{1.98}S_{0.02}$ electrode showed an excellent cycling performance, which is an unique characteristic of the layered manganese material, on the contrary to the previous reports.

Acknowledgements

This work is supported in part by the Ministry of Information and Communication of Korea (“Support Project of University Information Technology Research Center” supervised by KIPA).

References

[1] F. Capitaine, P. Gravereau, C. Delmas, Solid State Ionics 89 (1996) 197.
[2] A.R. Armstrong, P.G. Bruce, Nature 381 (1996) 499.
[3] I.J. Davidson, R.J. Mcllan, J.J. Murray, J.E. Greedan, J. Power Sources 54 (1995) 232.
[4] L. Croguennec, P. Deniard, R. Brec, J. Electrochem. Soc. 144 (1997) 3323.
[5] Y.-I. Jang, B. Huang, Y.-M. Chiang, D.R. Sadoway, Electrochem. Solid-State Lett. 1 (1998) 13.
[6] J.M. Paulsen, R.A. Donaberger, J.R. Dahn, Chem. Mater. 12 (2000) 2257.
[7] J.M. Paulsen, C.L. Thomas, J.R. Dahn, J. Electrochem. Soc. 146 (1999) 3560.
[8] T.E. Quine, M.J. Duncan, A.R. Armstrong, A.D. Robertson, P.G. Bruce, J. Mater. Chem. 10 (2000) 2838.
[9] J.P. Parant, R. Olazcuaga, M. Devalette, C. Fouassier, P. Hagenmuller, J. Solid Chem. 3 (1971) 1.
[10] K. Kubo, M. Fujiwara, S. Yamada, S. Arai, J. Power Sources 68 (1997) 553.
[11] A.R. Naghash, J.Y. Lee, Electrochim. Acta 46 (2001) 2293.
[12] A.R. Naghash, J.Y. Lee, Electrochim. Acta 46 (2001) 941.
[13] S.H. Park, K.S. Park, Y.-K. Sun, K.S. Nahm, J. Electrochem. Soc. 147 (2000) 2116.
[14] S.H. Park, Y.-K. Sun, K.S. Park, K.S. Nahm, Y.S. Lee, M. Yoshio, Electrochim. Acta 47 (2002) 1721.
[15] H.P. Klug, L.E. Alexander, X-ray Diffraction Procedure for Polycrystalline and Amorphous Materials, second ed., Wiley, New York, 1974.
[16] F. Lzumi, Nippon Kessho Gakkai Shi. 27 (1985) 23.
[17] M.R. Polacin, D. Larcher, A. Audemer, N. Sac-Epec, G.G. Amatucci, J.M. Tarascon, J. Electrochem. Soc. 144 (1997) 4226.
[18] L. Croguennec, P. Deniard, R. Brec, A. Lecerf, J. Mater. Chem. 1 (1995) 1919.
[19] A.D. Robertson, A.R. Armstrong, P.B. Bruce, Chem. Mater. 13 (2001) 2380.
[20] P.K. Sharma, G.J. Moore, F. Zhang, P. Zavalij, M.S. Whittingham, Electrochem. Solid-State Lett. 2 (1999) 494.
[21] G. Vitins, K. West, J. Electrochem. Soc. 144 (1997) 2587.
[22] T. Ohzuku, S. Kitano, M. Iwanaga, H. Matsuno, A. Ueda, J. Power Source 68 (1997) 646.